ARTICLE

Augmentation of inductive effects through short range intramolecular hydrogen bonds for the improvement of cooperativity of trimeric rosettes

Received 00th January 20xx,
Accepted 00th January 20xx

DOI: 10.1039/x0xx00000x

Andre Nicolai Petelski,*[a] Tamara Bundrea[a] and Nélida María Peruchena[b]

Cooperativity in hydrogen bonds can be crucial for the stabilization of supramolecular systems. In this contribution we propose a simple covalent modification within a pyrazole-based trimeric rosette that significantly improves its binding strength. Using dispersion-corrected density functional theory, at the BLYP-D3(BJ)/6-311++(d,p) level, we show how an intramolecular hydrogen bond acts as a bridge between an electron-donating and an electron-withdrawing group by moving electron density from one group to the other one through the sigma electron system. This effect strongly enhances the inductive ability of the substituents, and further increases the synergy of the cyclic trimer.

Design, System, Application

Based on a previously reported aminopyrazole rosette, we designed three new building blocks with improved cooperativity for the assembly of supramolecular trimeric rosettes. To this end, we combined three key principles: the direction of hydrogen bonds, the inclusion of electron-withdrawing (EW) and electron-donating (ED) groups and finally the inclusion of an intramolecular hydrogen bond. Through state-of-the-art dispersion-corrected density functional methods, including energy decomposition analysis, charge density descriptors and molecular orbital analyses, we show that the intramolecular hydrogen bond moves charge density from the EW group to the ED one. This translates into more negative charge on the acceptor side, and thus an enhanced cooperativity. We think this study opens a new road for the future synthesis of more robust self-assembled rosettes for obtaining one- and two-dimensional supramolecular materials, such as rosette nanowires and self-assembled monolayers, respectively.

Introduction

Hydrogen-bonded rosettes are receiving more reputation in supramolecular chemistry in the last years. One of its promising applications is the obtainment of non-covalent polymers by the spontaneous stacking of the rosettes.[1] Mastering the stability of these two levels of structures can be a challenging task for chemists. During the first step, the monomers must recognize themself in the right way to produce a cycle. Since hydrogen bonds (HBs) carry all the necessary information for the success of this step, it is essential to fully understand all the factors that modify and perturb these interactions. It is so that there have been a growing contribution dealing with the fine modulation of the HB. For example, the effects of the position of electron-withdrawing (EW) and donating groups (ED) on different dimers,[2] the effects of atom size within amides,[3] and the relative position of non-frontier atoms.[4] Other authors have demonstrated how chains of intramolecular HB,[5,6] which were made out of OH groups, can strengthen the donor ability of the terminal OH. The challenge faced by experimentalists is then how to rationally exploit this information to design a rosette structure.

The most common rosette structures are tetrameric, as in the guanine quadruplex[7] and other DNA derived macrocycles,[8] and hexameric.[9] We have demonstrated what is the source of stability in different tetrameric[10] and hexameric cyclic structures[11] and how to improve it.[12] Recently, it has been shown from experiments[13] and theory[14] how the length of the monomer impacts on the cooperativity of a tetrameric macrocycle. Nevertheless, the use of trimeric rosette is less usual in the literature and there are no studies about their cooperativity effects. The first cyclic trimer was reported by Zimmerman and Duerr.[15] Later Zimmerman et al.[16] also reported another trimeric rosette that self-organized with liquid crystal properties. In a work from 2008, Schrader et al.[17] have reported an extensive π-stacking of a trimeric rosette in water solution and in the crystal state. Since the authors pointed out that the HBs are not the main driving force for the final

[a] Departamento de Ingeniería Química, Universidad Tecnológica Nacional (UTN), Facultad Regional Resistencia (FRRe), CONICET, Centro de Investigación en Química e Ingeniería Teórica y Experimental (QUITEX), French 802, H3500CHJ, Resistencia, Chaco, Argentina.
[b] Laboratorio de Estructura Molecular y Propiedades (LEMyP), Instituto de Química Básica y Aplicada del Nordeste Argentino (IQUIBA-NEA), Consejo Nacional de Investigaciones Científicas y Técnicas, Universidad Nacional del Nordeste (UNNE-CONICET), Avenida Libertad 5460, 3400 Corrientes, Argentina.
† Footnotes relating to the title and/or authors should appear here.
Electronic Supplementary Information (ESI) available: [details of any supplementary information available should be included here]. See DOI: 10.1039/x0xx00000x

aggregation, it is evident that more knowledge on trimeric rosettes is needed.

In this work, we analyze the trimeric rosette reported by Scharder et al.[17] and further introduce three modifications with the purpose of significantly enhance the binding strength and cooperativity of the HBs. By using dispersion-corrected density functional theory, combined with energy decomposition analysis, molecular orbitals, and charge density descriptors, we show how combining three rational design principles can improve the self-assembling capabilities of specific trimer. First, the addition of EW and ED groups. Second, the arrangement of HBs pointing in the same direction, and, most importantly, the connection of the EW and ED groups via an ambifunctional HB to maximize their inductive effects.

Computational details

The trimeric rosette obtained by Schrader et al.,[17] which is based on an aminopyrazole-amino acid hybrid peptide, was used as a scaffold to apply our design principles. The skeleton of the structure is a pyrazole (P) ring, then at position 3 and 5 we used two types of substituents as shown in Figure 1. The structure of Schrader et al.[17] corresponds to the b-P35 monomer.

All monomers and trimers were then fully optimized with Gaussian 09,[18] by using the BLYP[19,20] functional with the refined version of Grimme dispersion (D3) and the Becke-Johnson[21] damping function (BJ). The empirical dispersion correction was implemented with the 3/124=40 IOp keyword. This functional has exhibited a great performance in similar hydrogen-bonded systems[11c-d,12] and in good accordance with experiments.[22] The electronic wave function was obtained with contracted gaussian-type orbitals[23] augmented with diffuse[24] and *d* and *p* polarization functions[25] by using the split valence 6-311+ +G(*d*,*p*) basis set.

The bonding energies of the trimeric rosettes (TR) were computed according to Eq. (1):

$$\Delta E_{bond} = E_{TR} - E_m \times 3 \qquad (1)$$

here, E_{TR} is the energy of the optimized TR and E_m is the energy of the isolated monomers.

The bonding energy was further dissected into deformation strain and interaction as shown in Scheme 1 (Eq. 2).

$$\Delta E_{bond} = \Delta E_{strain} + \Delta E_{int} \qquad (2)$$

The strain energy is the energy needed to deform the monomers from their isolated states (E_m) to the structure they acquire within the rosette ($E_{m\text{-}TR}$). As these deform structures are brought together to interact, the interaction energy is then obtained.

The cooperative energy of the systems was computed by comparing the interaction energy with the summation of all individual energy components (Eq. 3)

$$\Delta E_{syn} = \Delta E_{int} - \Delta E_{sum} \qquad (3)$$

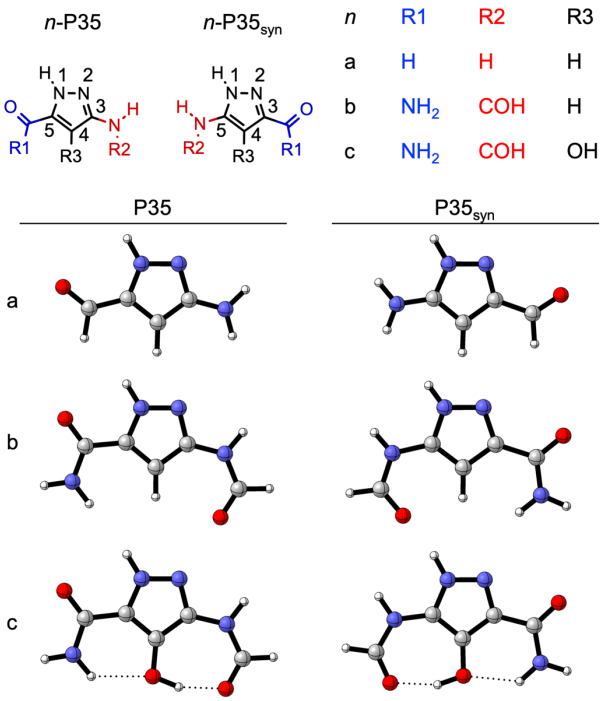

Figure 1. Molecular structure of selected monomers based on pyrazole (P) with covalent modifications at positions 3 and 5 (P35). The subindex syn indicates the monomers will show positive cooperativity or synergy.

The summation energy ΔE_{sum} (Eq. 4) is the addition of all interaction of the pairs within the rosettes computed by Eq. (5) (see also **Scheme 1**).

$$\Delta E_{sum} = 3 \cdot \Delta E_{pair} \qquad (4)$$

$$\Delta E_{pair} = E_{pair\text{-}TR} - E_{m\text{-}TR} \qquad (5)$$

The interaction energies of the trimers where then subjected to a localized molecular orbital energy decomposition analysis[26] (LMOEDA) at the same level of theory using the GAMESS[27] software. For the partition, each monomer was considered as a singular fragment. This method partitions the interaction energy into five components, according to Equation (8)

$$\Delta E_{int} = \Delta E_{elec} + \Delta E_{ex+rep} + \Delta E_{pol} + \Delta E_{disp} \qquad (8)$$

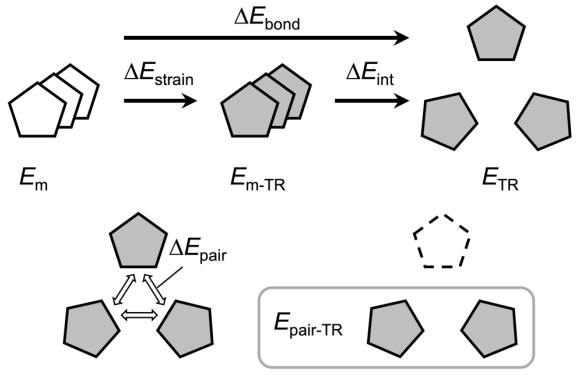

Scheme 1. Partition of the bond energy of trimeric rosettes (TR)

where the term ΔE_{elec} describes the classical electrostatic interaction (Coulombic) of the occupied orbitals of one monomer with those of another monomer; ΔE_{ex+rep} is the summation of the attractive exchange component resulting from the Pauli exclusion principle and the interelectronic repulsion; ΔE_{pol} describes the polarization and charge transfer components; and ΔE_{disp} corresponds to the dispersion term.

Molecular electrostatic potential surfaces (MEPS) for an isosurface of $\rho(r) = 0.001$ a.u., and the corresponding $V_{S,max}$ and $V_{S,min}$ values were computed with the Multiwfn software.[28] Voronoi deformation density (VDD) charges[29] on the monomers were also computed with the Multiwfn software.[28] All wave functions were obtained with the same level of theory. All figures were created with VMD,[30] CYLview,[31] Avogadro,[32] and Marvin.[33]

Results and discussion

Geometries and Bonding Analyses

Each trimer is bonded via two HBs: N–H···N and N–H···O. The geometrical parameters of these bonds are plotted in Figure 2, and they show two different patterns. In both systems, with and without cooperativity, the outer N–H···O hydrogen bonds are progressively shortened till reach a minimal distance of 2.697 Å. Regarding the inner N–H···N hydrogen bonds, they become longer when going from "a" to "b" trimers, and then they shorten again when going from "b" to "c" trimers, reaching similar values (2.9 Å) for the systems with and without cooperativity, as shown in Figure 2 (see also Table S3). The geometrical parameters of (b-P35)$_3$ trimer agree with those obtained from the experimental structure reported by Schrader et al.[17] The RMSD values computed for relevant geometric parameters are less than 0.1 Å (see Figure S1 in the Supporting Information file), indicating a very low deviation from the crystal structure.

The calculated bonding energies of all trimers are shown in Figure 3. Starting from (a-P35)$_3$, where donor and acceptor sites point in different directions, the ΔE_{bond} can be progressively enhanced. Within (b-P35)$_3$ trimer the ΔE_{bond} increases 4 kcal mol^{-1} when adding an ED group (–NH$_2$) on the donor side and an EW group (–COH) on the acceptor side of a-P35. Then, the inclusion of a –OH group at position 4 further increases the binding energy by 7.3 kcal mol^{-1}. This –OH group forms two HB with both substituents (see also Figure 1): N–H···O and O–H···O. The ΔE_{bond} thus go from –42.8 to –55.5 kcal mol^{-1} (see complete data set in Tables S1).

The (*n*-P35syn)$_3$ set of trimers (green, light blue, and blue) as shown in Figure 3, clearly shows that the systems can be further stabilized. This can be achieved by changing the position of the side groups (–COR1 and –NHR2) so that all HBs point in the same direction. This is a design principle that has been exploited for other Janus-type molecules.[34] However, the inclusion of the –OH group further increases the stability of the binding strength to –91.7 kcal mol^{-1}.

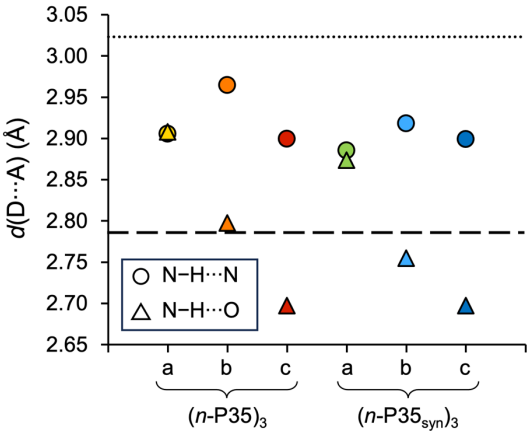

Figure 2. Average distances between donor (D) and acceptor (A) atoms corresponding to D–H···A hydrogen bonds: N–H···N (circles) and N–H···O (triangles). The dotted line and the dashed line indicate the average values of the N–H···N and N–H···O hydrogen bonds, respectively, corresponding to the crystal structure reported by Schrader et al.17

These computational experiments demonstrate that going from a-P35 to c-P35$_{syn}$ we could double the binding strength of the former cyclic trimer. As can be seen in Figure 3, the synergy of the last triad is also progressively improved, and it ranges from –12.6 to –17.4 kcal mol^{-1}. A reference system like the guanine quartet also shows a cooperative effect of –15 kcal mol^{-1} within the quadruplex.[35]

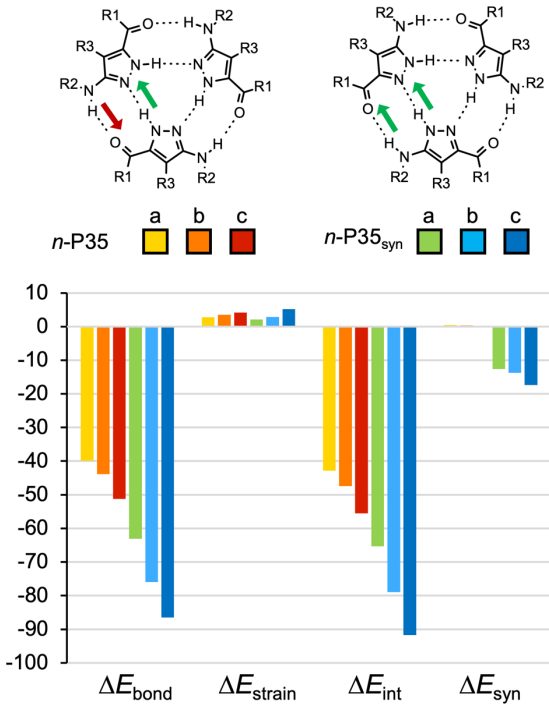

Figure 3. Bonding analysis (in kcal mol^{-1}) of trimeric rosettes computed at BLYP-D3(BJ)/6-311++G(d,p) level of theory. Interaction energies were corrected within the counterpoise procedure of Boys and Bernardi.[36]

To analyse the influence of the OH group without the formation of intramolecular HB, we added this substituent (R3) to (a-P35)$_3$ and (a-P35$_{syn}$)$_3$ trimers (see optimized structures in Figure S1). The interaction energies of these new trimers (a-P35*)$_3$ and (a-P35*$_{syn}$)$_3$ are –45.2 and –71.6 kcal mol^{-1} respectively and are –5.3 and –8.5 kcal mol^{-1} more stable than their original counterparts. This is, (a-P35*)$_3$ is 2 kcal mol^{-1} more stable than (a-P35)$_3$, while (a-P35*$_{syn}$)$_3$ is 6 kcal mol^{-1} more stable than (a-P35$_{syn}$)$_3$. More interestingly, all the HB distances were equalized, being 2.90 Å within the (1-P35*)$_3$ trimer and 2.85 Å within (1-P35*$_{syn}$)$_3$. This small experiment demonstrates that the OH group have a subtle influence by itself on the binding strength.

Nature of Bonding in Trimers

In this section, we decomposed the interaction energy of the trimers to analyse the nature of the gradual strengthening. To this end, we performed a LMOEDA and the values were plotted in Figure 4 (complete dataset can be found in the Supporting Information). From these results, polarization appears to govern the trend in interaction energies as they get more stabilizing. In lesser extent, the electrostatic component becomes more negative. As expected, the monomers get closer from a to c, and therefore the Pauli repulsion also increases, which is consistent with previous works.[11c-e,34] The term ΔE_{Pauli} as obtained with the EDA[37] scheme in ADF[38] is close to the sum of ΔE_{ex} + ΔE_{rep} obtained using the EDA scheme of the GAMESS program. It should be mentioned that both EDA schemes have shown similar outcomes in other systems.[39] Within the (n-P35)$_3$ systems, the dispersion term experiences an increase of about 1 kcal mol^{-1} from (a-P35)$_3$ to (b-P35)$_3$, and from (b-P35)$_3$ to (c-P35)$_3$. Within the (n-P35$_{syn}$)$_3$ systems, the increment is around 2 kcal mol^{-1} (see complete data set in Table S2).

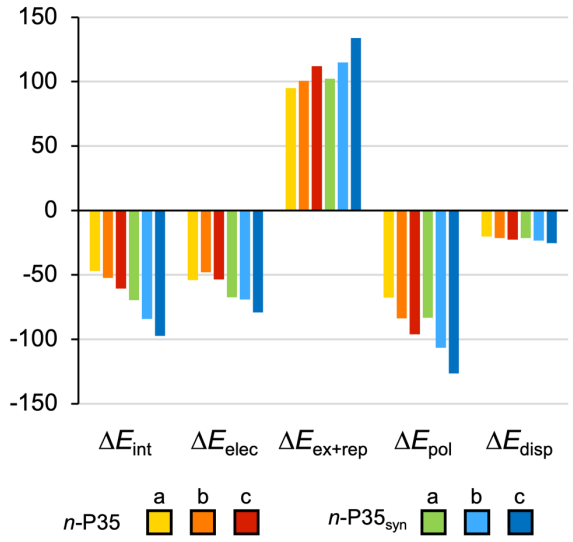

Figure 4. Local molecular orbital energy decomposition analysis (LMOEDA) of trimeric rosettes (in kcal mol^{-1}), computed at BLYP-D3(BJ)/6-311++G(d,p) level of theory.

Since electrostatic and orbital interactions are the main contributing components to the augmentation of the interaction energy, we can trace back why they increase systematically.

We first addressed the source of electrostatic by looking at the VDD charges over the frontier atoms, and the maxima and minima ($V_{S,max}$ and $V_{S,min}$) values over the MEPS.

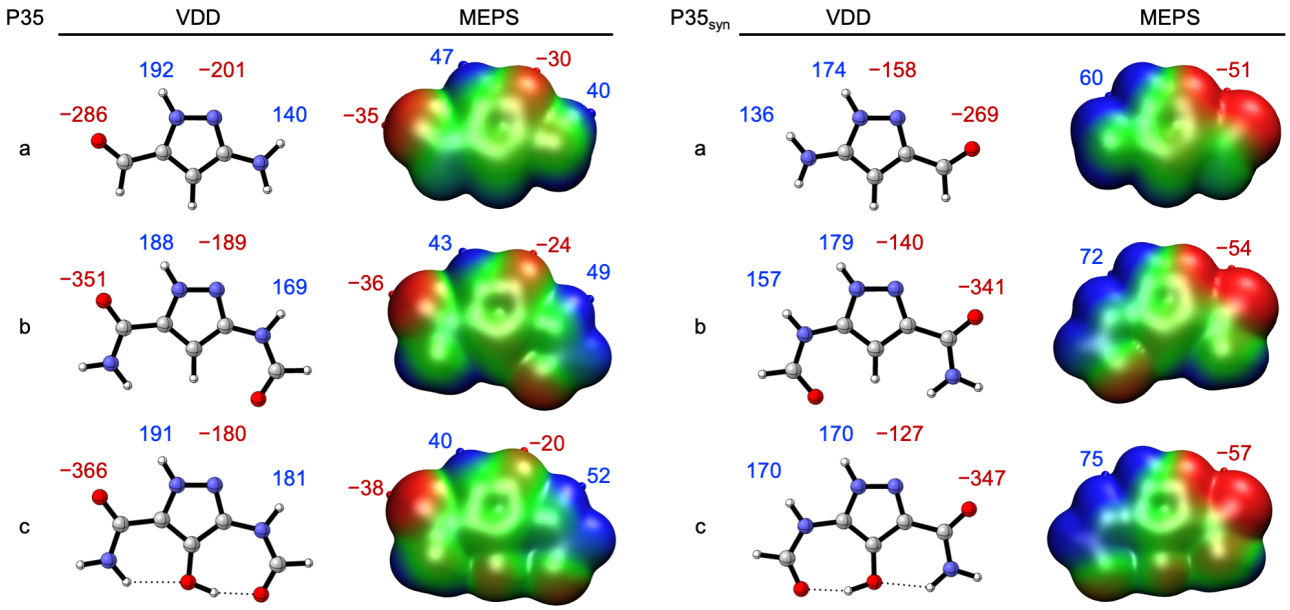

Figure 5. Voronoi deformation density (VDD) charges (in me$^-$) of the hydrogen atoms (blue values) and acceptor atoms (red values) of the isolated monomers, and molecular electrostatic potential surfaces (at 0.001 a.u.) from –0.05 (red) to 0.05 (blue) Hartree e^{-1} for the isolated monomers. Local maxima ($V_{S,max}$) and minima ($V_{S,min}$) are also indicated with blue and red spheres respectively with values in kcal mol^{-1}. All values were computed at BLYP-D3(BJ)/6-311++G(d,p) level of theory.

Figure 5 shows the VDD charges in milli-electrons of the equilibrium geometries along with their corresponding MEPS. Within the triad *n*-P35 the outer HB acceptor (O) and donor (H) atoms become more negative and positive respectively. The outer donor and acceptor sites become better partners to engage in HB interactions, and this explain the stronger electrostatic attraction. With regards to the inner HB donor atoms, the trend is opposite as they become less positively charged, while the inner HB acceptor atoms become less negatively charged. This means that the HB donor capability of N–H group is reduced HB, alike the HB acceptor capability of the endocyclic N.

The same effect can also be seen when analyzing the local maxima and minima of the MEPS. The $V_{S,min}$ on the outer O atom decreases from –35 to –38 kcal mol^{-1}, while the $V_{S,max}$ on the outer H atom increases from 40 to 52 kcal mol^{-1}. These observations are similar for the systems with cooperativity.

However, unlike other cooperative systems in which both frontier atoms experience either a gain or a reduction of charge density,[11c-e,34] the *n*-P35syn systems do not follow this trend. For instance, when looking the donor side, the outer HB donor becomes gradually more positive (the outer HB acceptor also becomes more negative), while the inner HB donor becomes gradually less positive (the inner HB acceptor also becomes gradually less negative). Therefore, the synergy might increase due to the stronger electrostatic attraction of the outer HB. As previously shown in Figure 2, the outer HB are the only ones that show a gradual decrease in distance.

Finally, the enhanced orbital interactions of the c-P35$_{syn}$ trimer are a natural effect of the charge separation between donor and acceptor sides. When moving from a-P35$_{syn}$ to c-P35$_{syn}$ the electrostatic pair interaction increases. The LUMO and LUMO+1 orbitals corresponding to the outer and inner σ^*_{N-H} antibonding, respectively, are stabilized because they become more positive (see Figures 5 and 6). On the other hand, the HOMO and HOMO–1 orbitals displayed in Figure 6 (lone pair of the outer O and endocyclic N atoms) are slightly destabilized in c-P35$_{syn}$ with respect to b-P35$_{syn}$ (the lone pair orbitals become more negative). The HOMO-LUMO gap therefore decreases by 0.29 eV from a-P35$_{syn}$ to c-P35$_{syn}$, leading to stronger donor-acceptor interactions.

Origin of the enhanced cooperativity

Now that we know why the individual electrostatic and polarization components gradually increase from *n* = a to c within each triad of rosettes, we want to analyze the role of the intramolecular hydrogen bond.

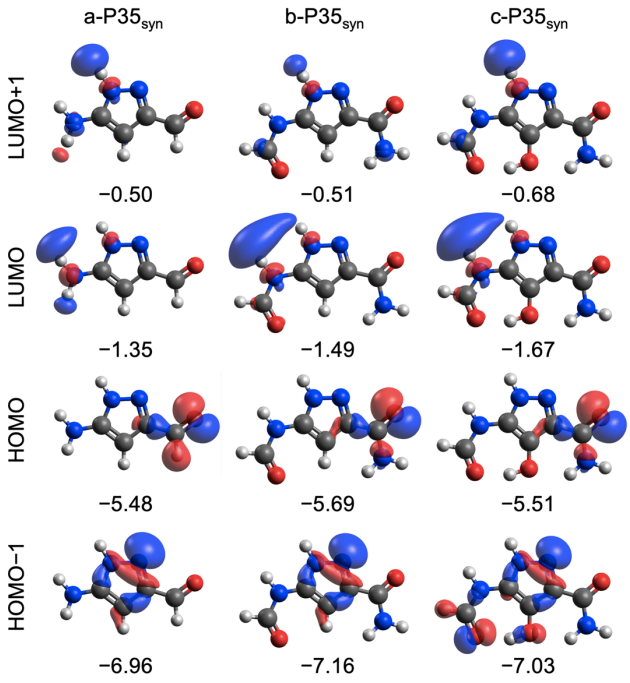

Figure 6. Isosurfaces (at 0.05 Bohr–3/2) and energies (in eV) of the σ orbitals of the isolated n-P35syn monomers that participate in hydrogen bonding interactions.

For this purpose, we compared the interaction energy of the (b-P35$_{syn}$)$_3$ trimer with that of (c-P35$_{syn}$)$_3$ but with its OH group rotated to break the intramolecular HB: (c-P35'$_{syn}$)$_3$. No geometry optimization was performed.

Figure 7 shows the VDD charges over the frontier atoms and the resulting interaction energies. The conformational rotation of the –OH group demonstrates that when the intramolecular HB is disrupted, the interaction energy of the trimer is almost the same as that in their counterpart without the OH group.

The energy difference between (2-P35$_{syn}$)$_3$ and (3-P35'$_{syn}$)$_3$ is only 1.3 kcal mol^{-1}. When the intramolecular interaction is turned on in (3-P35'$_{syn}$)$_3$, the interaction energy rises 12.8 kcal mol^{-1}. When looking at the changes in VDD charges follows that after the rotation of the –OH group and concomitant breakage of the HB, the VDD charge over the outer H become less positive. The VDD charge decreases from 170 me$^-$ to 158 me$^-$, thus its HB donor capability of the N–H group is lower. When the intramolecular HB is present, the carbonyl group donates electron density to the OH group (R_3) and the N–H group becomes more positive. Since the OH group (R_3) is forming an ambifunctional HB, it also donates charge density to the amine group.

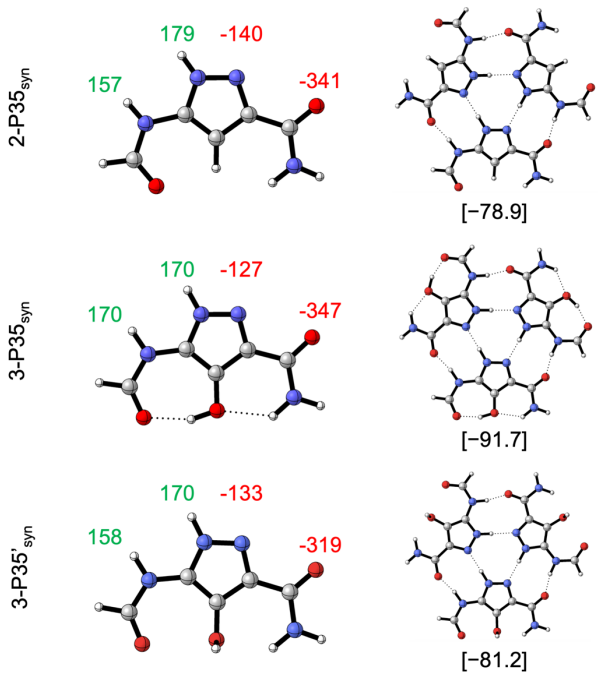

Figure 7. Left: Voronoi deformation density charges over the frontier atoms of 2-P35$_{syn}$, 3-P35$_{syn}$, and 3-P35'$_{syn}$ and their corresponding trimers (Right). Interaction energies (in kcal mol^{-1}) are shown between brackets.

Finally, this amine group donates again charge density to the frontier carbonyl group, as was previously shown within carboxamides.[3] Hence, the OH group is forcing the electron density to flow from one side of the molecule to the other side. Similar observations were found for a single water molecule in microhydrated structures of tetrahydrofuran.[40] When analyzing the transition b-P35$_{syn}$ → c-P35$_{syn}$ (see VDD charges in Figure 7) the frontier outer proton becomes more positive (from 157 to 170 me^{-}) and the frontier outer oxygen atom becomes more negative (from –341 to –347 me^{-}). To put in other words, their HB donor and acceptor capabilities are enhanced, respectively.

Conclusions

In summary, we have designed a trimeric rosette with an improved self-assembling capability by exploiting three key principles: cooperativity, inductive effects, and intramolecular hydrogen bonds. Our quantum chemical computations suggest that cooperativity can be enhanced not only by having all hydrogen-bond pointing in one direction, but also by adding electron donating substituents on the donor sites and electron withdrawing substituents on the acceptor sites. Furthermore, we have shown that if these two groups are interconnected by an intramolecular hydrogen bond the binding strength and cooperativity can be augmented. This enhancement effect can be understood in terms of electronic charge transfer through the sigma electron system. The intramolecular HB takes electron density from the electron-withdrawing group, and then it pushes this charge to the electron-donating one, thus increasing even more the charge accumulation on one of the frontier atoms. This translates into shorter outer hydrogen bonds, and stronger orbital interactions. The over-strengthened cooperativity is switched off by disrupting the intramolecular hydrogen bond with the solely rotation of the hydroxyl group.

Author Contributions

A.N.P. contributed to conceptualization, data curation, formal analysis, funding acquisition, investigation, methodology and writing – original draft. T.B. contributed to investigation and visualization. N.M.P. contributed to data curation, supervision, and writing – review & editing.

Conflicts of interest

There are no conflicts to declare.

Acknowledgements

National Scientific and Technical Research Council - Argentina (CONICET), and Secretaría de Ciencia y Técnología (SCyT) of the Universidad Tecnológica Nacional – Facultad Regional Resistencia (UTN – FRRe) of Argentine (Project No. ASPPARE0008387).

References

1 (a) K. Tamaki, T. Aizawaa and Shiki Yagai, *Chem. Commun.*, 2021, **57**, 4779; (b) A. Isobe, T. Kajitani and Shiki Yagai, *Angew. Chem. Int. Ed.*, 2023, **62**, e202312516; (c) C. Otsuka, S. Takahashi, A. Isobe, T. Saito, T. Aizawa, R. Tsuchida, S. Yamashita, K. Harano, H. Hanayama, N. Shimizu, H. Takagi, R. Haruki, L. Liu, M. J. Hollamby, T. Ohkubo and S. Yagai, *J. Am. Chem. Soc.*, 2023, **145**, 22563.
2 S. C. C. van der Lubbe, A. Haim, T. van Heesch and C. Fonseca Guerra, *J. Phys. Chem. A*, 2020, **124**, 9451.
3 C. Nieuwland and C. Fonseca Guerra, Chem. Eur. J., 2022, **28**, e202200755.
4 C. Nieuwland, D. Almacellas, M. M. Veldhuizen, L. de Azevedo Santos, J. Poater and C. Fonseca Guerra, *Phys. Chem. Chem. Phys.*, 2024, DOI: 10.1039/D3CP05244C.
5 N. Dominelli-Whiteley, J. J. Brown, K. B. Muchowska, I. K. Mati, C. Adam, T. A. Hubbard, A. Elmi, A. J. Brown, I. A. W. Bell and S. L. Cockroft, *Angew. Chem. Int. Ed.*, 2017, **56**, 7658.
6 L. Trevisan, A. D. Bond, C. A. Hunter, *J. Am. Chem. Soc.*, 2022, **144**, 19499.
7 J. T. Davis, *Angew. Chem. Int. Ed.*, 2004, **43**, 668
8 V. Váquez-González, M. J. Mayoral, R. Chamorro, M. M. R. M. Hendrix, I. K. Voets and D. González-Rodríguez, *J. Am. Chem. Soc.*, 2019, **141**, 16432.
9 A. Alenaizan, C. H. Borca, S. C. Karunakaran, A. K. Kendall, G. Stubbs, G. B. Schuster, C. D. Sherrill and N. V. Hud, *J. Am. Chem. Soc.*, 2021, **143**, 16, 6079.
10 A. N. Petelski, S. C. Pamies, A. G. Sejas, N. M. Peruchena and G. L. Sosa, *Phys. Chem. Chem. Phys.*, 2019, **21**, 8205.
11 (a) A. N. Petelski, N. M. Peruchena and G. L. Sosa, *J. Mol. Model.*, 2016, **22**, 202; (b) A. N. Petelski, N. M. Peruchena, S. C. Pamies and G. L. Sosa, *J. Mol. Model.*, 2017, **23**, 263; (c) A. N. Petelski and C. Fonseca Guerra, *ChemistryOpen*, 2019, **8**, 135; (d) A. N. Petelski and C. Fonseca Guerra, *J. Phys. Chem. C*, 2020, **124**, 3352; (e) A. N. Petelski and C. Fonseca Guerra, *Chem. Asian J.*, 2022, **17**, e202201010.

12 (a) A. N. Petelski, J. Marquez, S. C. Pamies, G. L. Sosa and N. M. Peruchena, *ChemPhysChem*, 2021, **22**, 665; (b) A. N. Petelski, S. C. Pamies, M. J. V. Marquez, G. L. Sosa and N. M. Peruchena, *ChemPhysChem*, 2022, **23**, e202200151.
13 C. Montoro-García, M. J. Mayoral, R. Chamorro and D. González-Rodríguez, *Angew. Chem. Int. Ed.*, 2017, **56**, 15649.
14 (a) D. Almacellas, S. C. C. van der Lubbe, A. A. Grosch, I. Tsagri, P. Vermeeren, J. Poater and C. Fonseca Guerra, *ChemistryEurope*, 2023, **2**, e202300036; (b) D. Almacellas, S. C. C. van der Lubbe, A. Grosch, I. Tsagri, P. Vermeeren, C. Fonseca Guerra and J. Poater, *Eur J. Org. Chem.* 2023, e202301164.
15 S. C. Zimmerman, and B. F. Duerr, *J. Org. Chem.*, 1992, **57**, 2215.
16 M. Suárez, J.-M. Lehn, S. C. Zimmerman, A. Skoulios and B. Heinrich, *J. Am. Chem. Soc.*, 1998, **120**, 9526.
17 P. Rzepecki, K. Hochdörffer, T. Schaller, J. Zienau, K. Harms, C. Ochsenfeld, X. Xie and T. Schrader, *J. Am. Chem. Soc.*, 2008, **130**, 586.
18 M. J. Frisch, G. W. Trucks, H. B. Schlegel, G. E. Scuseria, M. A. Robb, J. R. Cheeseman, J. A. Montgomery, T. Vreven, K. N. Kudin, J. C. Burant, J. M. Millam, S. S. Iyengar, J. Tomasi, V. Barone, B. Mennucci, M. Cossi, G. Scalmani, N. Rega, G. A. Petersson, H. Nakatsuji, M. Hada, M. Ehara, K. Toyota, R. Fukuda, J. Hasegawa, M. Ishida, T. Nakajima, Y. Honda, O. Kitao, H. Nakai, M. Klene, X. Li, J. E. Knox, H. P. Hratchian, J. B. Cross, V. Bakken, C. Adamo, J. Jaramillo, R. Gomperts, R. E. Stratmann, O. Yazyev, A. J. Austin, R. Cammi, C. Pomelli, J. W. Ochterski, P. Y. Ayala, K. Morokuma, G. A. Voth, P. Salvador, J. J. Dannenberg, V. G. Zakrzewski, S. Dapprich, A. D. Daniels, M. C. Strain, O. Farkas, D. K. Malick, A. D. Rabuck, K. Raghavachari, J. B. Foresman, J. V. Ortiz, Q. Cui, A. G. Baboul, S. Clifford, J. Cioslowski, B. B. Stefanov, G. Liu, A. Liashenko, P. Piskorz, I. Komaromi, R. L. Martin, D. J. Fox, T. Keith, A. Laham, C. Y. Peng, A. Nanayakkara, M. Challacombe, P. M. W. Gill, B. Johnson, W. Chen, M.W.Wong, C. Gonzalez and J.A.Pople, *Gaussian 09*, *Revision D.01*, Gaussian, Inc., Wallingford CT, 2004.
19 A. D. Becke, *Phys. Rev. A*, 1988, **38**, 3098.
20 C. Lee, W. Yang and R. G. Parr, *Phys. Rev. B*, 1988, **37**, 785.
21 S. Grimme, *J. Comput. Chem.*, 2004, **25**, 1463.
22 H. M. Coubrough, S. C. C. van der Lubbe, K. Hetherington, A. Minard, C. Pask, M. J. Howard, C. Fonseca Guerra and A. J. Wilson, *Chem. Eur. J.*, 2019, **25**, 785.
23 A. D. McLean and G. S. Chandler, *J. Chem. Phys.*, 1980, **72**, 5639.
24 T. Clark, J. Chandrasekhar, G. W. Spitznagel and P. V. R. Schleyer, *J. Comput. Chem.*, 1983, **4**, 294.
25 M. J. Frisch, J. A. Pople and J. S. Binkley, *J. Chem. Phys.*, 1984, **80**, 3265.
26 P. Su and H. Li, *J. Chem. Phys.*, 2009, **131**, 014102.
27 M. W. Schmidt, K. K. Baldridge, J. A. Boatz, S. T. Elbert, M. S. Gordon, J. H. Jensen, S. Koseki, N. Matsunaga, K. A. Nguyen, S. Su, T. L. Windus, M. Dupuis and J. A. Montgomery, *J. Comput. Chem.*, 1993, **14**, 1347.
28 T. Lu and F. Chen, *J. Comb. Chem.*, 2012, **33**, 580.
29 C. Fonseca Guerra, J.-W. Handgraaf, E. J. Baerends and F. M. Bickelhaupt, *J. Comput. Chem.*, 2003, **25**, 189.
30 W. Humphrey, A. Dalke and K. Schulten, *J. Mol. Graphics*, 1996, **14**, 33.
31 C. Y. Legault, *CYLview*, *1.0b*, Université de Sherbrooke, 2009, http://www.cylview.org.
32 *Avogadro*: an open-source molecular builder and visualization tool. Version *1.2.0*. http://avogadro.cc/; M. D. Hanwell, D. E. Curtis, D. C. Lonie, T. Vandermeersch, E. Zurek and G. R. Hutchison, *J. Cheminf.*, 2012, **4**,17.
33 Marvin 19.13.0, 2019, ChemAxon (http://www.Chemaxon.Com).
34 D. Almacellas, C. Fonseca Guerra and J. Poater, *Org. Biomol. Chem.*, 2023, **21**, 8403.
35 C. Fonseca Guerra, H. Zijlstra, G. Paragi and F. M. Bickelhaupt, *Chem. Eur. J.*, 2011, **17**, 12612.
36 S. F. Boys and F. Bernardi, *Mol. Phys.*, 1970, **19**, 553
37 (a) T. Ziegler and A. Rauk, *Inorg. Chem.*, 1979, **18**, 1755; (b) F. M. Bickelhaupt and E. J. Baerends, in *Reviews in Computational Chemistry*, eds. K. B. Lipkowitz and D. B. Boyd, Wiley-VCH, New York, 2000, vol. 15, p. 1-86.
38 (a) G. te Velde, F. M. Bickelhaupt, E. J. Baerends, C. Fonseca Guerra, S. J. A. van Gisbergen, J. G. Snijders and T. Ziegler, *J. Comput. Chem.*, 2001, **22**, 931; (b) ADF2019.102, SCM Theoretical Chemistry; Vrije Universiteit, Amsterdam, The Netherlands, www.scm.com.
39 (a) N. Thellamurege and H. Hirao, *Molecules*, 2013, **18**, 6782. (b) R. Wysokiński, *Phys. Chem. Chem. Phys.*, 2022, **24**, 12860.
40 M. M. Vallejos and N. M. Peruchena, *J. Phys. Chem. A*, 2012, **116**, 4199.